Hindawi
Advances in Civil Engineering
Volume 2024, Article ID 5538831, 11 pages
https://doi.org/10.1155/2024/5538831

Research Article

Evaluating the Effect of Cement and ARG Fiber on the Mechanical and Microstructural Properties of Dune Sand

Faisal I. Shalabi[1], **Javed Mazher**[2], **Kaffayatullah Khan**[3], **Muhammad Nasir Amin**[3], **Mesfer Alqahtani**[3], **Hosam Awad**[3], **Ali Alghannam**[3] and **Hussain Albaqshi**[3]

[1]*Department of Civil Engineering, Hijjawi for Engineering Technology, Yarmouk University, Irbid, Jordan*
[2]*Physics Department, College of Science, King Faisal University, Al-Ahsa, Saudi Arabia*
[3]*Department of Civil Engineering, College of Engineering, King Faisal University, Al-Ahsa, Saudi Arabia*

Correspondence should be addressed to Faisal I. Shalabi; faisal.shalabi@yu.edu.jo

Received 19 June 2023; Revised 21 December 2023; Accepted 20 January 2024; Published 2 February 2024

Academic Editor: Zhen-Jun Wang

Despite its collapsible nature and weakness, desert sand can be used for construction purposes all over the world if properly stabilized. Therefore, the aim of this study is to evaluate the effectiveness of cement and fiber in stabilizing locally available dune sand. A test plan was used to investigate the effects of varying quantities of alkali resistance glass (ARG) fiber (F: 0%, 0.2%, 0.4%, and 0.6%) and portland cement (C: 0.0%, 1.0%, 3.0%, and 5.0%) on the mechanical and microstructural properties of dune sand. Mechanical properties such as unconfined strength (UCS), strain at failure (ε_f), California bearing ratio (CBR), and modulus of elasticity (E_s) were evaluated, and microstructure properties were investigated using Raman spectrum and laser-scanning microscopy (LSM) tests on stabilized sand samples. The results of the experimental study showed that the percentage of cement in the treated sand has a more significant impact on the investigated properties of the treated sand than the percentage of fibers. In addition, increasing fiber content results in an increase in the ductility of the sand mix. Raman analysis revealed significant interactions between sand mix components. Moreover, LSM results showed that fiber–cement interaction increased with increasing cement percentage, as calcium silicate hydrates (CSH) formed in the mix and filamentous and intrastrand binding occurred. The findings of this study indicate that ARG fiber and cement can be effective in the stabilization of dune sand for construction purposes even with the use of low percentages of ARG fiber (0.2%–0.4%) and cement (3%).

1. Introduction

In large countries with spacious desert areas and with the need to develop and build an extended highway and railway network, the availability of construction materials that possess the required engineering properties becomes a real challenge. To fulfil this need, countries need to extensively use construction materials from quarries. The great use of natural materials from quarries is expected to impair the environment. Many countries and construction companies start to explore the possibility of using dune sand as construction materials to overcome the above mentioned issues. Dune sand is mainly classified as fine and poorly graded materials. Besides that, it has loose and collapsible structure with low strength and cohesion that make it not suitable for construction of foundations of roads and buildings. But it might have good potential use in construction if properly treated or reinforced with stabilizers to enhance its engineering properties that fulfil the project requirements and specifications.

Researchers globally investigated the effect of adding different additives and stabilizers on the behavior of dune sand. In fact, among the different materials that can be used to stabilize dune sand, cement and lime have proven to be the most effective [1, 2]. In this part of the study, the authors attempt to highlight the most common materials used to stabilize due sands and their impact on the mechanical properties of the sand mix. Shalabi et al. [2] developed practical relationships among CBR value, UCS, and elastic modules of lime-volcanic ash stabilized dune sand. Smaida et al. [3] used cement, pozzolan, and lime to improve the strength of desert sand in flexible pavement. Lopez-Querol et al. [4] studied the impact of cement on Jeddah Aeolian dune sand. The work

outcomes indicated that the bearing capacity of the stabilized sand increases by increasing the cement content, and it is independent of the compaction energy. Elsawy [5] investigated the behavior of dune sand stabilized with different percentages of cement. The results showed that the maximum dry density increases with the increase in cement content leading to a reduction in porosity and optimum moisture content. Albusoda and Salem [6] used cement kiln dust (CKD) as stabilizer for sandy soils. The outcomes indicated a significant financial and structural capability to stabilizing collapsing soils. For example, when 8% CKD is added, the final bearing capacity increases to 250%. The UCS and bearing resistance of treated waste sand demonstrated an increase with higher cement content and prolonged curing time. Remarkably, the addition of just 2% cement significantly enhances the technical qualities of the waste sand, and also, practical correlations were observed between the UCS, CBR value, and initial tangent modulus of waste sand treated with cement [7]. When ordinary portland cement, OPC/CBPD (cement by-pass dust), is introduced to sand, it significantly enhances both cohesiveness and friction angle. The addition of OPC results in a threefold increase in cohesion and friction angle compared to the use of CBPD alone [8]. The optimal mix design for utilizing stabilized dune sand as a foundation soil or in highway road layers was achieved mostly at 3% cement content. Prolonged curing durations further contribute to an additional enhancement in the bearing capacity of the stabilized dune sand. Many investigations have indicated that, in the absence of stabilizer in Aeolian sand, Aeolian sand exhibited CBR value of almost 4%. However, incorporating 10% cement and 15% geopolymer resulted in CBR values of 133% and 112%, respectively [5].

Recently, fibers and polymeric materials were introduced by many researchers to reinforce soils for possible use in construction works. Liu et al. [9] utilized a mixed of polymeric fibers and polyurethane organic polymer to stabilize and reinforce sand. The results showed that the maximum UCS is achieved with a mix composition of 0.3% fiber and 4% polymer. Liu et al. [10] used organic polymer and fiber to stabilize sand. The results showed that the highest value of cohesion is obtained at a mix of 4% polymer and 0.6% fiber. Mohsin and Attia [11] used polymeric solution to stabilize the sand surface and improve the wind resistance erosion. The results indicated that, as the polymer percentage increases, the tensile resistance and modulus of the mix increase. Rezaeimalek et al. [12] explored the influence of activated polymer on the stabilization of SP sands. The work outcomes demonstrated that, for the same polymer/water ratio, as the amount of polymer increases, the strength of the treated sand increases, and the optimal ratio of polymer to water is found to be 2 : 1. On the other hand, fiber also stands out as the most frequently employed material for soil stabilization/strengthening and is also efficient in enhancing liquefaction resistance, strength, and the capacity to restrict swelling potential. Bayoumy et al. [13], based on the results of experimental tests, concluded that the UCS of the clayey sand increases with the addition of polypropylene fibers or portland cement. However, at high stresses, fibers exhibit more ductile compressive performance, whereas the cemented samples display an abrupt brittle failure. Al-Refeai and Al-Suhaibani [14] found that incorporating polypropylene fiber as a stabilizer in dune sand increased CBR values, maintaining a higher range of penetration compared to natural state dune sand. An optimal result was achieved with approximately 0.4% by weight of fiber content. A study by Chahar and Prasad [15] showed that using 1.5% by weight of Recron fiber has proven to be effective for the stabilization of dune sand. Yetimoglu and Salbas [16] explored the influence of fiber content on the strength of sands. The outcomes of the study showed that the peak strength of the treated sand is not influenced by the fiber content. However, the residual strength and ductility significantly improved with the presence of fiber. Ibrahim et al. [17] explored the effect of using flexible fiber on the liquefaction characteristics of loose clean sand. The results showed that the presence of randomly oriented fibers reduced the liquefaction potential. Jiang et al. [18] used short polypropylene fibers to improve the properties of soils. The results showed that the addition of fibers improved both the UCS and the angle of internal friction of the treated soil. Onyejekwe and Ghataora [19] studied the impact of randomly distributed discrete fibers on the properties of the cohesive soils. The results indicated that the presence of discrete fibers in the mixture considerably increased the toughness and residual strength of the stabilized soil. Tang et al. [20] investigated the influence of randomly distributed fibers on the soil capacity. The outcomes of the results revealed that the peak and residual strength of the stabilized soil significantly improved with addition of fibers. Maher and Woods [21], based on torsional shear tests on fiber-reinforced sand, found that the dynamic shear modulus increased with the increase in both the fiber content and aspect ratio.

In the literature review, no studies have been identified related to the combined use of cement and ARG fiber for the stabilization of dune sand. Therefore, in this study, Type V portland cement with ARG fiber was used to enhance the characteristics of the dune sand for possibility application in engineering construction. Different percentages of portland cement (0, 1%, 3%, and 5%) and ARG fiber (0, 0.2%, 0.4%, and 0.6%) were used. Conventional tests were initially conducted to characterize and classify the dune sand. UCS and CBR tests were conducted to evaluate the impact of cement–fiber reinforcement on the mechanical properties of the treated dune sand including CBR, UCS, and E_s. Results of LSM and Raman spectrum tests combined with that of the mechanical tests were used to analyze the interaction among the mixture components and to explain the stabilization mechanism. As a result, practical and helpful relationships were established among UCS, E_s, and CBR that can be implemented for the design of the base and subbase of roads and foundations of structures using a mixture of dune sand–cement–fiber as construction materials.

2. Utilized Materials

2.1. Dune Sand. Sand was gathered from a construction company in Al-Ahsa region in Saudi Arabia. Originally, the material located in huge quantities along Al-Ahsa-Dammam road. Figures 1(a) and 1(b) show the used dune sand. The

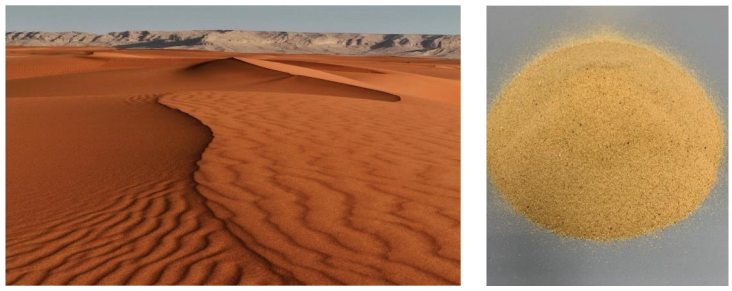

(a) (b)

Figure 1: (a) Dune sand, east of KSA, and (b) a close photo of used sand.

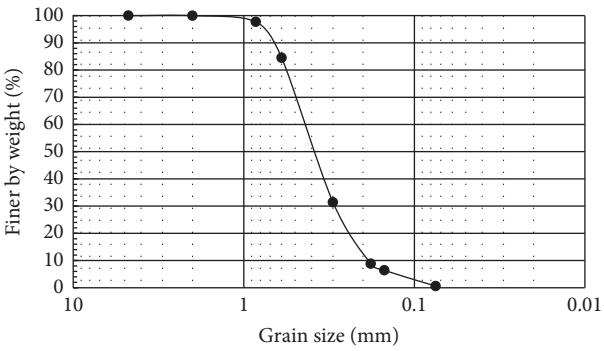

Figure 2: Grain size distribution of the dune sand.

Table 1: Properties and classification of the utilized sand.

Soil property/classification system	Value/description
Specific gravity, G_s	2.69
Color	Yellow
Coefficient of curvature, $C_C = D^2_{30}/D_{10}\, D_{60}$	1.18
Coefficient of uniformity, $C_u = D_{60}/D_{10}$	2.50
Shape of grains	Rounded–subrounded
Unified soil classification system, USCS	SP sand
AASHTO	A3 material

classification tests showed that the sand is considered as SP and A3 according to the USCS System [22, 23] and AASHTO system [24], respectively. The grain size distribution showed that the sand is falling in the size range of 0.1–0.9 mm (with $D_{50} = 0.45$ mm), as shown in Figure 2. The fundamental properties and classification of the dune sand are shown in Table 1.

2.2. Alkali Resistance Glass, ARG Fiber. In this work, 22 mm in length ARG glass fiber was used. The fiber has a high percentage of zirconia (ZrO_2), and it has the following advantages: never rusts, noncombustible, has high reinforcing performance, and can easily be mixed with earth materials [25], which makes it a good stabilizer candidate for dune sand. Figure 3 shows a sample of ARG fiber while Table 2 shows its properties.

2.3. Cement and Water. Type V portland cement was used in this study. It is widely used in the construction of structures

Figure 3: Sample of 22 mm in length ARG fiber.

Table 2: Properties of alkali resistance glass (ARG) fiber [25].

Property	Value
Thermal expansion coefficient	9×10^{-6}/°C
Softening point	830°C
Densify	2.8 g/cm^3
Tensile strength	1.5 GN/m^2
Young's modulus	74 GN/m^2
Strain at failure	2%
Alkali resistivity (weight loss)	0.8%
Acid resistivity (weight loss) Held at 80°C for 90 hr. in 10% HCL	1.6%

subjected to high level of sulfates such as pavement concrete, roads foundation, sidewalks, and reinforced concrete structures. According to the tests performed previously at the laboratory of King Faisal University on the same type of cement used in this study, the results showed that the cement has different types of oxides with the majors: CaO (63.7%) and SiO_2 (21.2%). Besides that, the cement has major chemical compounds: C_3S (59%), C_2S (16%), and C_4AF (14.6%) with average initial setting time of 155 min. and fineness of 306 m^2/kg [7].

Water used in the mix was provided by KFU desalination unit. According to ASTM C1602 [26], the water has less than 10,000 ppm of chlorides, less than 3000 ppm of sulfates, less than 15,000 ppm of dissolved salts, and pH around 7.5.

3. Testing Plan and Methodology

3.1. Physical and Mechanical Tests. A testing scheme was designed and performed to fulfill the goals of this task. The

Table 3: Detailed testing plan of the stabilized dune sand.

Test/(standard)	Percentage of cement by weigh of dry sand	Percentage of fiber by weight of dry sand
Bulk Sp. Gr., G_s ASTM D854 [30]	0	0
GSD (ASTM D6913)	0	0
Standard proctor (ASTM D698-07)	0	0
USCS classification (ASTM D2487-17) AASHTO classification (AASHTO M 145-82)	0	0
UCS (ASTM D2166-85)-A	0, 1, 3, 5	0.0, 0.2, 0.4, 0.6
CBR value (ASTM D1883-07)-C	0, 1, 3, 5	0.0, 0.2, 0.4, 0.6

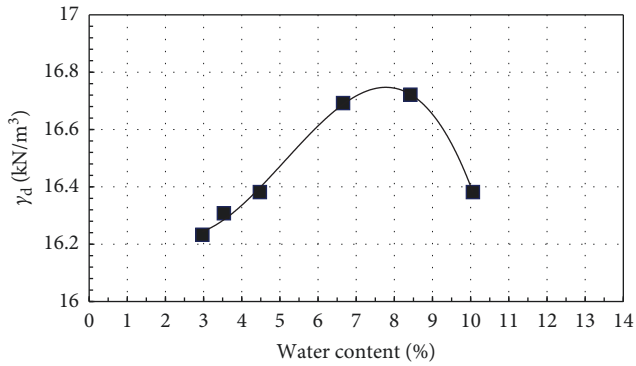

Figure 4: Standard proctor compaction curve of the dune sand.

scheme focused on exploring the mechanical properties and behavior of dune sand stabilized at different percentages of cement (0.0%, 1.0%, 3.0%, and 5.0%) and ARG fiber (0.0%, 0.2%, 0.4%, and 0.6%). Cement and fiber were mixed with sand and compacted at the optimum moisture content (OMC) and maximum dry unit weight (γ_{damx}) of the sand using standard Proctor ASTM D698-07-A [27]. To fulfil the objectives of the work, two main tests were considered, namely: UCS and CBR, following ASTM D2166-85 [28] and ASTM D1883-07 [29] standards, respectively. All sand-mix samples were tested after 28 days of curing time. Table 3 presents the conducted testing program. Figure 4 shows the compaction curve of the dune sand with OMC and γ_{damx} of 7.7% and 16.9 kN/m^3, respectively.

3.2. Micro-Raman Spectroscopy. Horiba's Labram Evolution-2 spectrometer is used to record the Raman spectra at 633 nm wavelength red laser (He-Ne) excitation source. Before the sample recording, the spectrometer is first calibrated using the 520.7 cm^{-1} Raman peak of the standard Si-311 crystal. Throughout the Raman confocal measurements, the confocal hole is kept at fixed hole size of 50 airy units (1 a.u. = $1.22 \times \lambda$/numerical aperture). The spectral data are recorded at fixed grating of size 1,800 line/inch giving the spectral accuracy of 0.5 cm^{-1}.

3.3. Laser Scanning Microscopy. Zeiss's LSM-800 confocal laser scanning microscope is used to capture the morphologies of the samples of fiber–cement mixtures. A focused laser beam of wavelength 405 nm is used to scan over the sample, and the reflected intensity of laser is collected as a function of position to create a digital image of the reflected light. The morphologies are recorded both at high-resolution imaging using 50x objective lens and wide area imaging 5x lens giving scan areas of 200 μm and 2 mm, respectively. The LSM noise is significantly reduced through the confocal image data acquisition mode deploying the confocal hole of size ~ 1 A.U., where 1 Airy-unit $\approx 1.22 \times \lambda$/NA, and numerical aperture of objective lens is ~ 1.41.

3.4. Statistical Modeling. Two-way ANOVA method, which is the analysis of variance in response function with respect to the multiple treatment factors, is used to statistically evaluate the effectiveness and interaction of ARG fiber and portland cement treatments of the fiber-reinforced sand-mix samples [2]. Four-level treatments are applied on the sand mixture, four weight-percentage values of ARG fiber and portland cement are considered, respectively, and the variances in UCS, E_s, and CBR mechanical responses are studied. Coefficient of variance, which is the ratio of the explained (treatment) variance to unexplained (error) variance, is calculated for both the treatment and interaction variances. The coefficient of variance can be computationally obtained using a statistical data analysis software [31]. Probability of obtaining the ratio, P value, which is the measure of confidence in the null hypothesis (ineffective treatment), can also be calculated from the software. The P value ≤ 0.05 indicates a statistical significance of the treatment factor or interaction among the factors used in the study.

4. Results and Discussions

4.1. Raman Spectroscopy. The ARG fibers used in the current studies are composite glass fibers and have a typical composition ratio of 15–20 wt.% of Zirconia (ZrO_2) and 80–85 wt.% of silica (SiO_2) mixed phase. The presence of zirconia imparts the characteristic alkali-resistive traits to these glass fibers [32]. Raman spectrum is employed to identify the composition phases present in the chopped strands of the as-procured ARG fibers, as shown in Figure 5(a). Characteristic Raman peak of the silica phase is observed at 526 cm^{-1} in the fiber strand confirming the strong presence of the silica-related compositional phase in the strand [33]. The characteristic mode is related to the breathing vibration of the SiO_2. Further, a strong peak related to SiO_2 glasses is obtained at 975 cm^{-1} related to the Si-O stretching modes [34]. The presence of the later peak is confirmatory to the SiO_2 glassy phase in the ARG

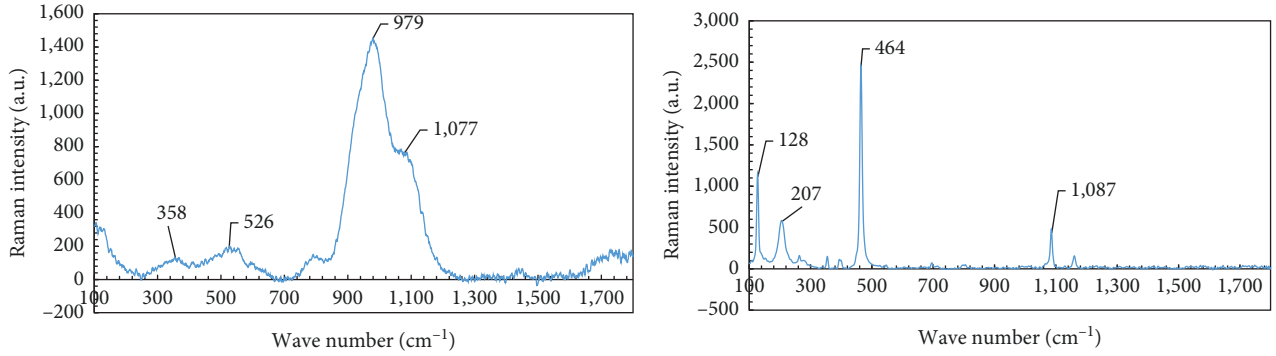

(a) (b)

Figure 5: (a) Raman spectrum of the ARG fiber the characteristic peaks of the zirconia (357 cm^{-1}) and silica (526 cm^{-1}) and (b) raman spectrum of the Portland cement and the calcium silicate peaks (464 and 1,087 cm^{-1}).

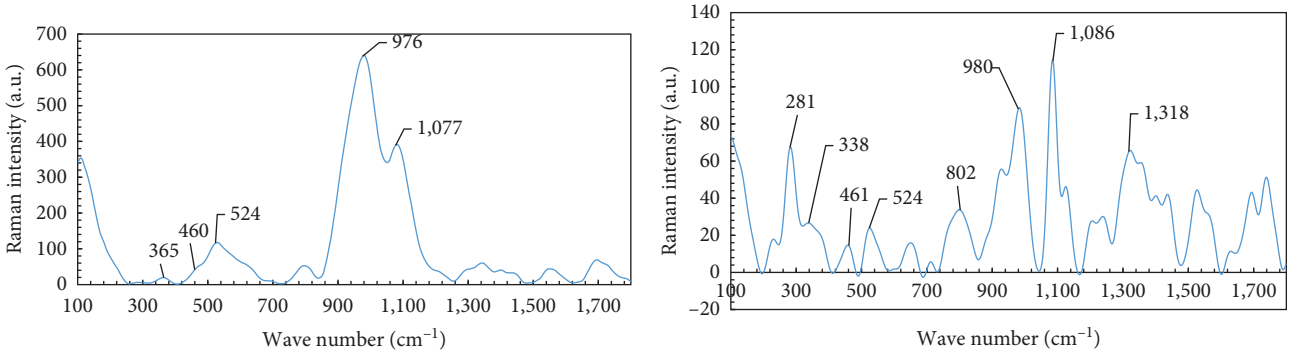

(a) (b)

Figure 6: (a) Raman spectrum of the concrete sample with 3 wt.% of cement and 0.6 wt.% of fiber and (b) raman spectrum of the concrete sample with 5 wt.% of cement and 0.6 wt.% of fiber.

fiber strand. Remaining two distinguished peaks of the spectrum at 358 cm^{-1} are related to the metal oxide's characteristic peak confirming the presence of the tetragonal phase of zirconia in the fiber. The peak of 1,077 cm^{-1} is possibly related to the expected formation of the solid solution phase also known as zircon ($ZrSiO_4$) in the as-procured fibers, and that could be present owing to the use of high-temperature processes used during the manufacturing of ARG fibers [35, 36]. Thus, the three distinguished phases of the ARG fiber strand, easily identifiable in the Raman studies, are silica, zirconia, and zircon phases.

The portland cement's major components, lime and limestone phases, are observed at 464 and 1,087 cm^{-1} spectral positions, respectively, in its Raman spectrum, which is shown in Figure 5(b). The peak corresponding to 464 cm^{-1} relates to the air sintered lime, and that is one of the major component comprising 70 wt.% in the portland cement's composition [37]. Similarly, a strong Raman signature peak positioned at 1,087 cm^{-1} is attached to the calcite (calcium carbonate) phase of the portland cement [38]. The peak has also been frequently reported in the literature as a principal wavenumber of the limestone's Raman mode [39]. The peaks at 128 and 207 cm^{-1} positioned at the lower energy range of the spectra are typically the traits of high-temperature-processed portland cement, in which the formation of wollastonite phase ($CaSiO_3$) takes place at higher manufacturing temperatures >1,100°C via diffusion of lime and silica components of cement [40].

Figure 6(a) represents the Raman spectrum of the concrete sample in which the dune sand grains are mixed with 3 wt.% of portland cement and 0.6 wt.% of ARG fiber strands. The Raman characteristic peak of the fiber's zirconia phase is observed to be shifted to 364 cm^{-1} on mixing with the cement from its pure phase position of 358 cm^{-1} indicating a possibility of small chemical interaction of fibrous phase with that of the cement phase in the mortar. Similarly, any noticeable shift is not observed in the zircon phase of the fiber, which remains at the position of 1,077 cm^{-1} indicating that the zircon phase remains chemically unperturbed in the mortar in this sample. Raman signals of the silica phase in the sand mix do not provide any imperative chemical information since the signals are not distinct to the fiber itself and originate from all the components of the sand mix, and moreover, no shift in its positions at 520 and 980 cm^{-1} is observed. The portland cement's characteristic lime phase is also detected with the help of a shoulder at 460 cm^{-1}.

However, on increasing the portland cement concentration to 5 wt.% (Figure 6(b)), a number of new peaks arise along with the strengthened signal of the lime-related Raman mode at 461 cm^{-1}, indicating increase in the mortar's cement ratio. Concurrently, a large shift of 27 cm^{-1} in the Raman

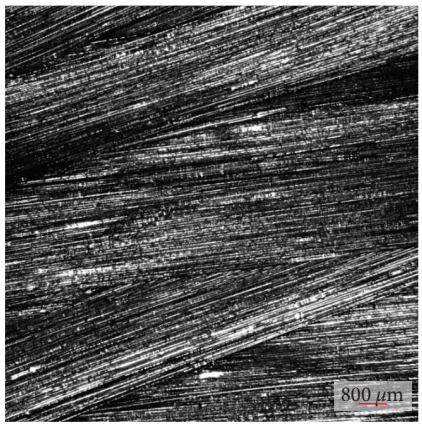

Figure 7: Laser scanning image of as-procured ARG fibers without any wet processing. Red colored scale ≈ 800 μm length.

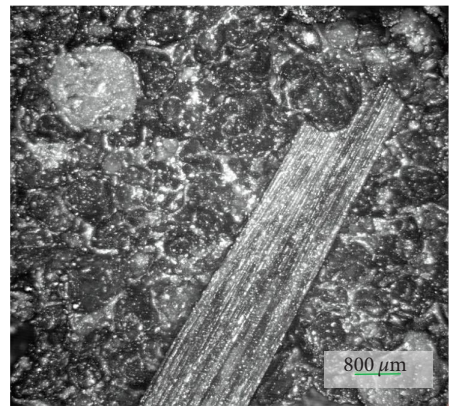

Figure 8: Laser scanning image of the sand mix comprising of 3% Portland cement and 0.6% fiber strands. Green colored scale ≈ 800 μm length.

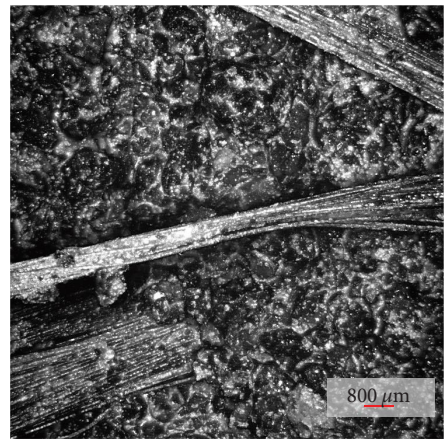

Figure 9: Laser scanning image of the sand mix comprising of 5% Portland cement and 0.6% fiber strands. Red colored scale ≈ 800 μm length.

position of zirconia phase is observed, and that is shifted from the position of 365 cm^{-1} in the as-procured fiber strands to 338 cm^{-1} in the sand mix sample manifesting a strong interaction in between zirconia and cement phases of the sand mix. The stronger interaction on increasing the fiber content can be deciphered from recent reports on the presence of zirconium oxide molecules deaccelerating the hydration process of the concrete and thus making the hydration products more uniformly distributed and denser restricting the growth space for calcium hydrate crystals [41]. Moreover, the presence of Zirconia has also been reported to affect both mechanical and thermal properties of the cement pastes [41]. A confirmation of fiber–cement chemical interaction can also be deciphered from a small but noticeable shift of the zircon peak from 1,077 to 1,086 cm^{-1}. A prominent peak at 281 cm^{-1} is indicative of appearance of limestone $CaCO_3$ phase in the mortar on increasing the cement concentration to 5% [42]. Raman signals of slaked lime, $Ca(OH)_2$ or calcium hydroxide, also appeared in the samples with higher cement reinforcement and can be identified by a Raman peak positioned at 802 cm^{-1} [43]. Another marker of strong chemical interaction between the sand mix components, sand, fiber, and cement in the sample with high cement ratio is the calcium silicate hydrate (CSH) formation due to the binding of lime with silica, and that is observed in the form of new Raman peaks around 1,318 cm^{-1} [44].

4.2. Laser Scanning Microscopy. The as-procured ARG fibers are shown in Figure 7. The fibers are forming the filamentous strands and observed to be grouped together in the strands of length of 5–7 cm and the strand diameter of several millimeters, typically 2–3 mm. Further, it is clear from the image that every fiber strand further comprises several tens of bundled filaments, and each of the filament has uniform diameter throughout its length. Throughout the sample morphology, all the filaments are tightly and homogeneously packed in the fiber strand. A fixed filament diameter of ≈100 μm is observed in all the fiber stands, and that can also be deciphered from the LSM image.

Morphology of the sand mix having 3% cement is shown in Figure 8 depicting a fibrous top surface of the composite sample. A compact top morphology of the sample originates from the adhesive interaction of cement with the dune sand grains and the fiber strands. It is clear that the fibers are well buried inside the concrete, which indicates that fiber strands are adhesively bonded to the mortar and a chemical interaction of cement–fiber is present in the sand mix. However, the results do not show any intrastrand adhesion among the fiber strands, and that may be due to the smaller cement ratio in the concrete. Moreover, no cement residues are observed on the dispersion of filaments covering the strands.

On increasing the cement concentration in the sand mix, a further compact morphology is observed as shown in Figure 9. All the components of the sand mix are well adhered, and fibers can be seen as intermingled together. Moreover, some cement residue can be clearly found on top of the fiber strands indicating excellent wetting of filaments in the mortar and appearance of intrastrand binding. Please note that the as-purchased ARG fibers strands always come in with filaments agglomerated together. Though the filament diameter is much smaller, the overall fiber strand has thickness of 100 μm, and that is also mentioned in the ARG specifications from the supplier [25]. The filamentous binding as observed in the

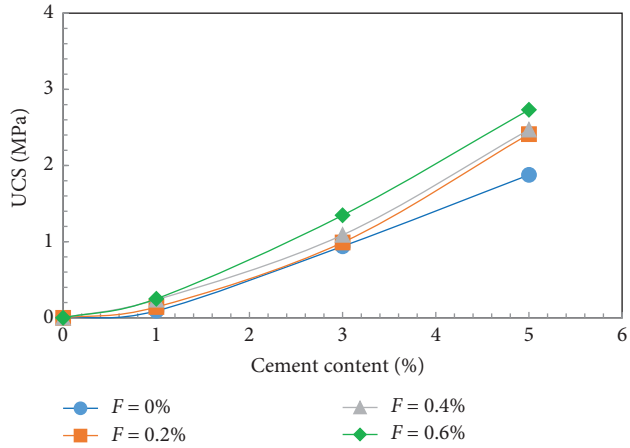

FIGURE 10: UCS vs. cement content of the stabilized dune sand for different % of fiber.

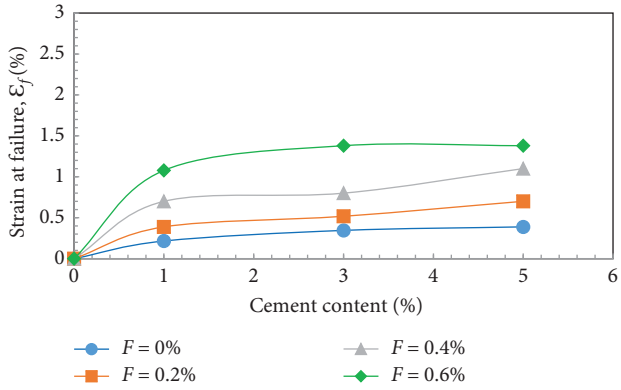

FIGURE 11: Strain at failure vs. cement content of the stabilized dune sand for different % of fiber.

sample can further provide additional strength to the sand mix. The stronger interaction among the sand mix components has also been observed in the Raman studies in Section 4.1 and Figure 6(b).

4.3. UCS and ε_f of the Sand Mix. Results of the UCS and ε_f of the stabilized sand mix at different ARG fiber and cement contents are shown in Figures 10 and 11, respectively. The tested sample were prepared at the OMC and γ_{dmax} of the sand compacted at standard Proctor compaction effort. Different percentages of cement (0.0%, 1.0%, 3.0%, and 5.0%) and ARG fiber (0.0%, 0.2%, 0.4%, and 0.6%) were mixed with the sand. The samples were 116 mm in height and 102 mm in diameter. Each sample was tightly wrapped and sealed by fine nylon film and stored 28 days for curing at room at a temperature between 21 and 23°C. The outcomes in Figure 10 indicate that the UCS increases with the increase in contents of both fiber and cement. The effect of cement content on the increase in UCS is obvious as a result of forming calcium silicate hydrate gel (CSH) that tends to coat the sand grains and develop strong bonds at the contact points [44]. Introducing ARG fiber in the cement–sand mix has different effects. As can be seen in Figure 10, at the same cement content, as the percentage of ARG fiber increases, the UCS increases. This behavior is more obvious at high percentages of cement content, and it can be explained by the results obtained by Raman spectra analysis for high cement content ($C = 5\%$, Figure 6(b)), which showed the development of new peaks (at 461 cm^{-1}) and shift in the zircon peaks of ARG fiber (from 365 cm^{-1} for 3% cement to 338 cm^{-1} for 5% cement and from 1,077 cm^{-1} for 3% cement to 1,086 cm^{-1} for 5% cement), manifesting the stronger interaction between zirconia and cement phases of the treated sand. Also, the results of LSM provided a strong evidence on the impact of fiber–cement interaction on the increase in the UCS of the stabilized sand as the cement content increases. By increasing the cement content, LSM results (Figure 9) showed that all the fibers adhere to the mix in an intermingled packing and compact morphology. Besides that, the image in the same figure showed some residue of cement on the top of fiber strands indicating of the appearance of intrastrand bindings which provide an additional strength to treated dune sand.

The impact of fiber and cement contents on the strains at failure (ε_f) of the sand mix is shown in Figure 11. The results show that, at the same cement content, as the fiber content increases, the ε_f increases. The effect of cement on ε_f is relatively small for cement content greater than 1%. The presence of fiber in the sand mix has a significant effect on the ε_f, and obviously, it converted the behavior of the treated sand mix to be more ductile as its percentage in the mix increases. Figures 12 ((a), 12(b), 12(e), and 12(f)) show that, for low percentages of fiber ($F = 0\%$ and 0.2%), the specimens under compression showed almost one-crack pattern, while for higher percentages of fiber (0.4% and 0.6%), many failure surface were developed and distributed all over the specimen body (multicracks pattern), as shown in Figures 12 ((c), 12(d), 12(g), and 12(h)).

4.4. E_s of the Sand Mix. Results of E_s at different cement and ARG fiber contents are demonstrated in Figure 13. The outcomes in this figure indicate that E_s increases with the increase in cement content. The increase in E_s with the increase in cement content is attributed to the CSH formation as the lime in the cement interact with the silica of the sand, leading to a strong chemical interaction among the sand grains. On the other hand, the results in the figure indicate that, as the percentage of the fiber increases, E_s decreases. As discussed in Section 4.3, the increase in fiber content tends to enhance the ductility of the sand mix as more cracks are developed and widely distributed over the volume of the tested sample, and as a result, the stiffness decreases. The effect of fiber content on E_s decrease is maximum at a cement content of 3%. At this cement content, the sand mix lost more than 50% of its E_s value when the fiber content increased from 0% to 0.6%. By using cement content of 5%, the results in Figure 13 demonstrate that there is a very minor effect of the fiber on the E_s of the sand mix, and in this case, it can be concluded that the cement has almost the major effect on E_s.

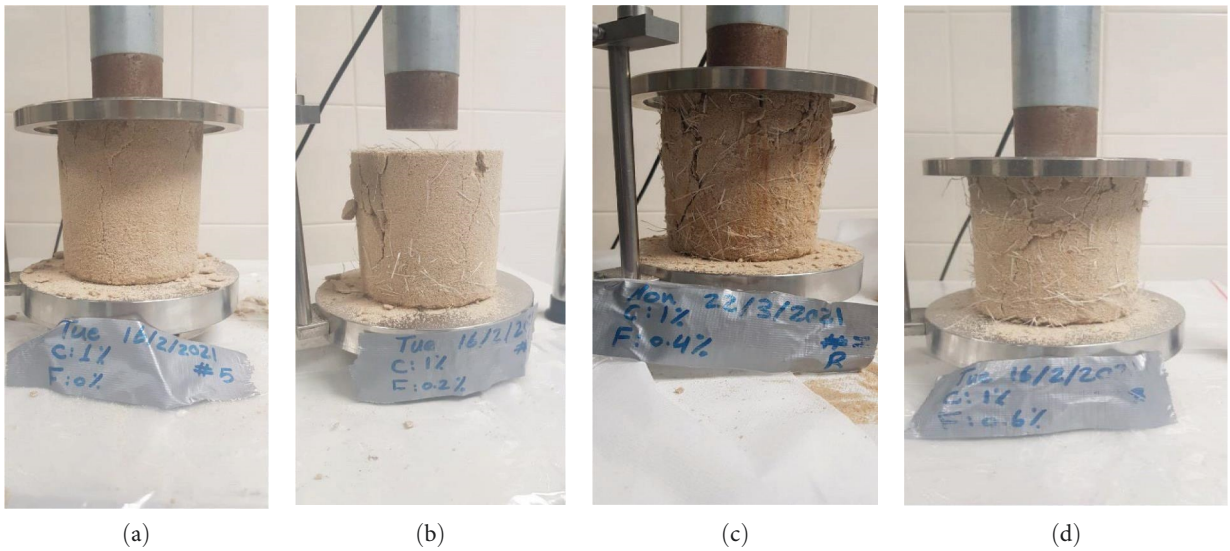

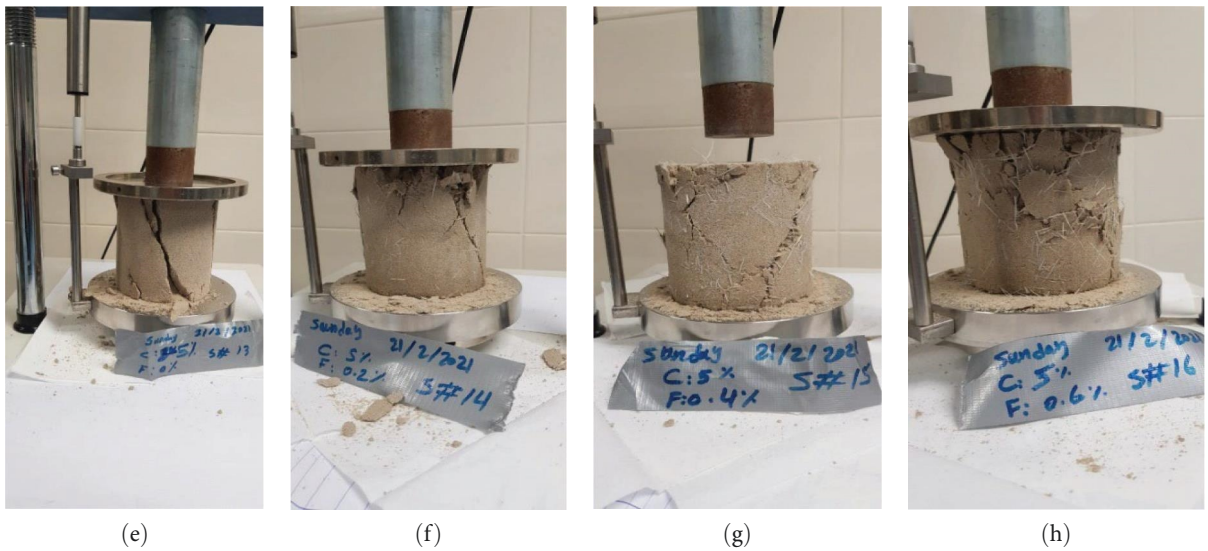

FIGURE 12: Craks distribution in samples tested for unconfined compression with cement content, C of 1% (samples: (a–d)) and cement content, C of 5% (samples: (e–h)) mixed with different precentages of ARG fibers ($F = 0\%$, 0.2%, 0.4%, and 0.6%).

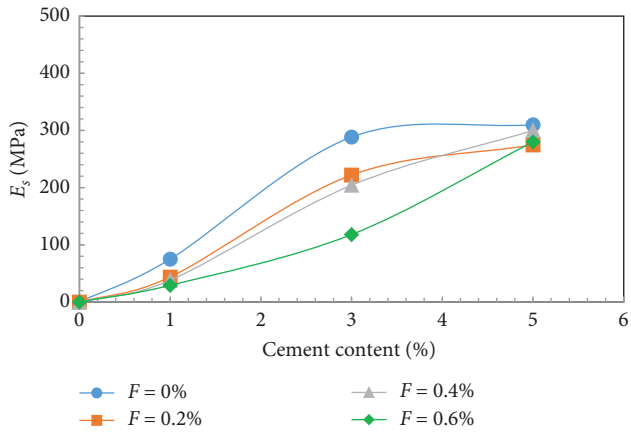

FIGURE 13: E_s vs. cement content of the stabilized dune sand for different % of fiber.

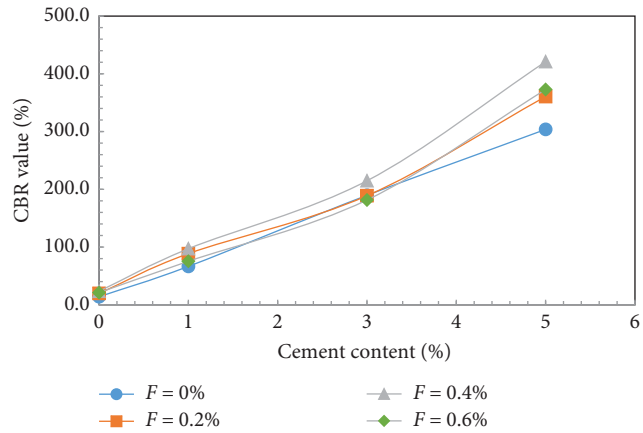

FIGURE 14: CBR value vs. cement content of the stabilized dune sand for different % of fiber.

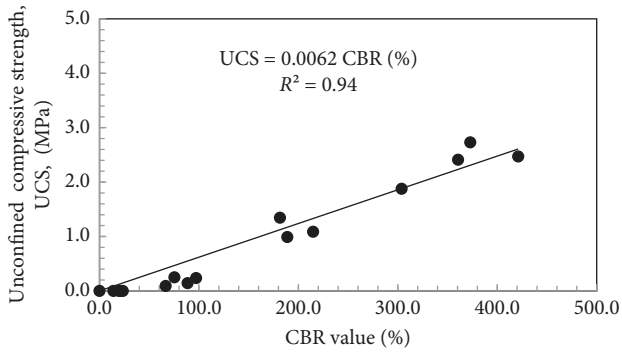

Figure 15: UCS vs. CBR value of the stabilized dune sand.

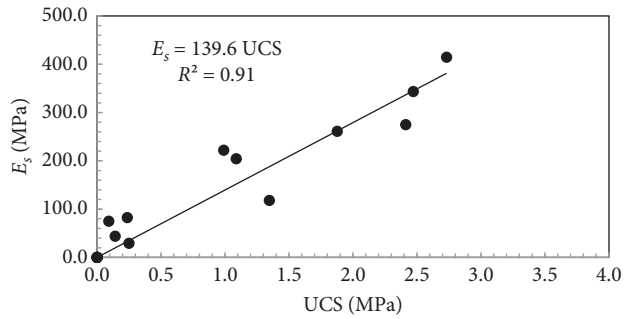

Figure 16: E_s vs. UCS of the stabilized dune sand.

4.5. CBR Value of the Sand Mix. CBR tests were conducted on the sand mix at the same conditions utilized for the strength tests. The outcomes in Figure 14 indicate that, for the same fiber content, CBR intensifies as the cement content increases. This behavior, as discussed in Section 4.4, is mainly attributed to the interaction between the lime cement and the silica in sand and the development of robust bonds at the contact points of the grains as the CSH gel coats the sand grains, leading to a higher CBR values. For the effect of ARG fiber on CBR value, Figure 14 shows that, at low cement content (0%–3%), there is almost no effect. For higher cement content (greater than 3%), the results in general show that, at higher percentages of fiber content, almost higher values of CBR are obtained. This behavior is almost consistent with what has been observed on the effect of fiber on UCS, and the interpretation of the results is almost identical for both.

4.6. Valuable and Practical Relationships. The tests of UCS and CBR at different percentage of cement and ARG fiber contents led to a development of simple, useful, and practical relationships that can be used in the engineering design practice. Figure 15 represents a powerful linear relation between UCS (MPa) and CBR value (%). The relation can be simply expressed as UCS = 0.0062 CBR with correlation coefficient, $R^2 = 0.94$. Figure 16 represents the relation between E_s (MPa) and UCS (MPa). The relation can also be expressed in a linear form as $E_s = 139.6$ UCS with correlation coefficient, $R^2 = 0.91$. Finally, Figure 17 represents the relation between E_s (MPa) and CBR value (%), which as well can be simply expressed in a linear form as $E_s = 0.89$ CBR with correlation coefficient, $R^2 = 0.93$.

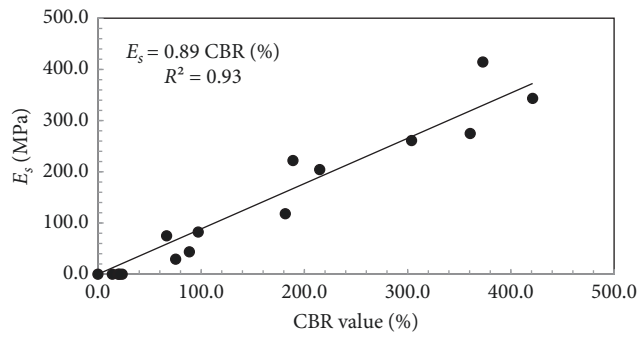

Figure 17: E_s vs. CBR value of the stabilized dune sand.

4.7. Statistical Analysis. The two-factor ANOVA calculations give different P values for the two cement and fiber factors, 0.000038 and 0.056, respectively, for the results of UCS indicating that the effect of cement on the composite strength is much stronger than that of the fiber. Moreover, the change in the fiber concentration is a weaker factor since its P value is more than the cutoff level of significance ~0.05.

For the results of E_s, the ANOVA analysis generated P values 0.00013 and 0.114 for the cement and fiber concentrations, again indicating that the modulus depends strongly on the cement concentrations and the fiber concentration is a weaker factor. ANOVA analysis on the elasticity results indicate a relatively higher P values for both cement and fiber, 0.005 and 0.93, respectively, indicating that elasticity of the dune sand mix composite is not effectively controlled by both the cement and fiber compositions.

CBR test's ANOVA analysis indicates a good dependence of the ration on cement concentration but a weaker dependency on the fiber's presence in the composite. The P value (1×10^{-8}) for the cement treatment in the sand mix is much smaller than the cutoff level of significance indication excellent control of CBR by cement composition. However, the P value (0.079) for fiber treatment in the sand mix is slightly higher that the cutoff significance indicating its weaker effect on the CBR values of the sand mix.

5. Conclusions

Experimental scheme was executed to explore the impact of utilizing ARG fiber and cement as additives on the mechanical properties and behavior of dune sand as construction materials for foundations of roads and structures. The scheme consists of two main sections. The first section focused on the chemical information and morphology of sand–cement–fiber. The second section explored the mechanical characteristics of the sand mixture. The results of the first section were used to interpret and explain the findings of the second section. Based on the outcomes, the following conclusions were extracted:

(1) Micro-Raman spectroscopy is effectively deployed to identify the presence of zirconia and silica phases in the ARG fibers with the help of respective positions of their characteristic vibrational modes. The presence of a third zircon phase, which is a high-temperature solid solution phase of the two former phases, is also detected in the ARG fibers. The typical portland

cement identification is also performed by the Raman spectra, and usual calcite and wollastonite phases are detected in the cement. Raman analysis also indicates a significant interaction of the components of the sand mix composites; Raman shifts are observed in the characteristic peaks of the fibrous phase indicating the zirconia's interaction with the cement.

(2) The interaction between the fiber and cement phases in the sand mix is also found to increase with the increase in cement content due to the formation of CSH phases in the sand mix. ARG fibers of 100 μm diameter are observed morphologically in the LSM imaging, and filament is found to be longitudinally grouped together in strands of thickness 2–3 mm indicating a good porosity of fibers.

(3) Test results demonstrate that sand mixes with higher cement, and fiber contents have higher UCS and CBR while lower E_s. By increasing the cement content from 1% to 3%, the UCS increases from 0.2 to 1.2 MPa (600% increase) and the CBR value increases from 80% to 200% (250% increase). At cement content of 3% and by increasing the fiber content from 0% to 0.6%, the UCS increases from 0.8 to 1.4 MPa (175% increase), while the CBR value has no significant change with the fiber content increase. The observed decrease in E_s with the increase in fiber content is mainly due to enhancing the ductility of the sand mix as more cracks are developed through the volume of the tested samples during the loading process. The effect of fiber content on E_s decrease is found to be maximum at a cement content of 3%.

(4) The presence of fibers has pronounced effect on the sand mixes deformation behavior. As the fiber content increases, the sand mix shifts from a brittle to a more ductile mode, and more cracks were observed through the body of the samples. For example, at a cement content of 1% and by increasing the fiber content from 0% to 0.6%, the ε_f increases from 0.2% to 1.1% (550% increase). With the absence of fiber, the results indicate that the cement content has almost no effect on ε_f.

(5) A valuable and practical relationship with high correlation coefficients was established among UCS, CBR, and E_s of the sand mixes with varying amounts of cement and ARG fiber. These relationships are expected to be useful for the design processes of foundations of roads and buildings when the cement–fiber–dune sand is used as a construction material.

(6) The two-factor ANOVA results indicate that cement concentration strongly impacts the mechanical properties of sand mix composites, while fiber addition has less impact on UCS, E_s, and CBR properties.

Data Availability

The data used to support the findings of this study are available upon reasonable request directed to the corresponding author.

Conflicts of Interest

The authors declare that there are no conflicts of interest.

Acknowledgments

The authors acknowledge the Departments of Civil Engineering and Physics at KFU, Al-Hofof, KSA, for executing the experimental program in their laboratories.

References

[1] S. K. Tiwari, J. P. Sharma, and J. S. Yadav, "Behaviour of dune sand and its stabilization techniques," *Journal of Advanced Research in Applied Mechanics*, vol. 19, no. 1, pp. 1–15, 2016.

[2] F. I. Shalabi, J. Mazher, K. Khan et al., "Influence of lime and volcanic ash on the properties of dune sand as sustainable construction materials," *Materials*, vol. 14, no. 3, Article ID 645, 2021.

[3] A. Smaida, S. Haddadi, and A. Nechnech, "Improvement of the mechanical performance of dune sand for using in flexible pavements," *Construction and Building Materials*, vol. 208, pp. 464–471, 2019.

[4] S. Lopez-Querol, J. Arias-Trujillo, M. GM-Elipe, A. Matias-Sanchez, and B. Cantero, "Improvement of the bearing capacity of confined and unconfined cement-stabilized Aeolian sand," *Construction and Building Materials*, vol. 153, pp. 374–384, 2017.

[5] M. B. D. Elsawy, "Geotechnical behavior of stabilized dunes sand by cement," *Journal of Civil Engineering and Construction*, vol. 10, no. 2, pp. 69–74, 2021.

[6] B. S. Albusoda and L. A. K. Salem, "Stabilization of dune sand by using cement kiln dust (CKD)," *Journal of Earth Sciences and Geotechnical Engineering*, vol. 2, no. 1, pp. 131–143, 2012.

[7] F. Shalabi, J. Mazher, K. Khan et al., "Cement-stabilized waste sand as sustainable construction materials for foundations and highway roads," *Materials*, vol. 12, no. 4, Article ID 600, 2019.

[8] M. Al-Aghbari and R. Dutta, "Effect of cement and cement bypass dust on the engineering properties of sand," *International Journal of Geotechnical Engineering*, vol. 2, no. 4, pp. 427–433, 2008.

[9] J. Liu, Q. Feng, Y. Wang, Y. Bai, J. Wei, and Z. Song, "The effect of polymer-fiber stabilization on the unconfined compressive strength and shear strength of sand," *Advances in Materials Science and Engineering*, vol. 2017, Article ID 2370763, 9 pages, 2017.

[10] J. Liu, Y. Bai, Q. Feng et al., "Strength properties of sand reinforced with a mixture of organic polymer stabilizer and polypropylene fiber," *Journal of Materials in Civil Engineering*, vol. 30, no. 12, 2018.

[11] M. A. Mohsin and N. F. Attia, "Inverse emulsion polymerization for the synthesis of high molecular weight polyacrylamide and its application as sand stabilizer," *International Journal of Polymer Science*, vol. 2015, Article ID 436583, 10 pages, 2015.

[12] S. Rezaeimalek, J. Huang, and S. Bin-Shafique, "Evaluation of curing method and mix design of a moisture activated polymer for sand stabilization," *Construction and Building Materials*, vol. 146, pp. 210–220, 2017.

[13] M. Bayoumy, M. El Sawwaf, A. Nasr, and A. Elsawwaf, "Strength characteristics of clayey sand stabilized using polypropylene fiber or Portland cement," *Transportation Infrastructure Geotechnology*, vol. 2, no. 4, pp. 427–433, 2008.

[14] T. Al-Refeai and A. Al-Suhaibani, "Dynamic and static characterization of polypropylene fiber-reinforced dune sand," *Geosynthetics International*, vol. 5, no. 5, pp. 443–458, 1998.
[15] V. Chahar and C. D. Prasad, "Stabilization of sand dunes with recron fiber and cement kiln dust," *ECS Transactions*, vol. 107, no. 1, pp. 5693–5702, 2022.
[16] T. Yetimoglu and O. Salbas, "A study on shear strength of sands reinforced with randomly distributed discrete fibers," *Geotextiles and Geomembranes*, vol. 21, no. 2, pp. 103–110, 2003.
[17] E. Ibraim, A. Diambra, D. Muir Wood, and A. R. Russell, "Static liquefaction of fibre reinforced sand under monotonic loading," *Geotextiles and Geomembranes*, vol. 28, no. 4, pp. 374–385, 2010.
[18] H. Jiang, Y. Cai, and J. Liu, "Engineering properties of soils reinforced by short discrete polypropylene fiber," *Journal of Materials in Civil Engineering*, vol. 22, no. 12, pp. 1315–1322, 2010.
[19] S. Onyejekwe and G. S. Ghataora, "Effect of fiber inclusions on flexural strength of soils treated with nontraditional additives," *Journal of Materials in Civil Engineering*, vol. 26, no. 8, 2014.
[20] C.-S. Tang, D.-Y. Wang, Y.-J. Cui, B. Shi, and J. Li, "Tensile strength of fiber reinforced soil," *Journal of Materials in Civil Engineering*, vol. 28, no. 7, 2016.
[21] M. H. Maher and R. D. Woods, "Dynamic response of sand reinforced with randomly distributed fibers," *Journal of Geotechnical Engineering*, vol. 116, no. 7, pp. 1116–1131, 1990.
[22] ASTM D6913, *Standard Test Methods for Particle-Size Distribution (Gradation) of Soils Using Sieve Analysis*, ASTM: West Conshohocken, PA, USA, 2017.
[23] ASTM D2487, *Standard Particle for Classification of Soils for Engineering Purpose (Unified Soil Classification System)*, ASTM: West Conshohocken, PA, USA, 2017.
[24] AASHTO M145-82, *Standard Specification for Classification of Soils-Aggregate Mixtures for Highway Construction Purposes*, AASHTO, Washington, DC, USA, 1991.
[25] "Glass fiber, nippon electric glass," Accessed May, 2021, https://www.neg.co.jp/en/product/fiber/.
[26] ASTM C1602, *Standard Water for Concrete*, ASTM: West Conshohocken, PA, USA, 2006.
[27] ASTM D698-07, *Standard Test Methods for Laboratory Compaction Characteristics of Soils Using Standard Effort*, ASTM: West Conshohocken, PA, USA, 2007.
[28] ASTM D2166-85, *Standard Test Method for Unconfined Compressive Strength of Cohesive Soil*, ASTM: West Conshohocken, PA, USA, 2013.
[29] ASTM D1883-07, *Standard Test Method for CBR (California Bearing Ratio) of Laboratory-Compacted Soils*, ASTM: West Conshohocken, PA, USA, 2007.
[30] ASTM D854, *Standard Test Methods for Specific Gravity of Soils by Water Pycnometer*, ASTM: West Conshohocken, PA, USA, 2014.
[31] "Microsoft-Excel's Data Analysis-ToolPak software version," 2021.
[32] E. Mader, R. Plonka, M. Schiekel, and R. Hempel, "Coatings on alkali-resistant glass fibers for the improvement of concrete," *Journal of Industrial Textiles*, vol. 33, no. 3, pp. 191–207, 2004.
[33] E. Berrier, C. Zoller, F. Beclin, S. Turrell, M. Bouazaoui, and B. Capoen, "Microstructures and structural properties of sol–Gel silica foams," *The Journal of Physical Chemistry. B*, vol. 109, no. 48, pp. 22799–22807, 2005.
[34] M. Ivanda, R. Clasen, M. Hornfeck, and W. Kiefer, "Raman spectroscopy on SiO_2 glasses sintered from nanosized particles," *Journal of Non-Crystalline Solids*, vol. 322, no. 1–3, pp. 46–52, 2003.
[35] M. Mansoor, M. Mansoor, M. Mansoor, Z. Er, K. Czelej, and M. Ürgen, "Can stress-induced changes in phonon frequencies of $ZrSiO_4$ make it a potential IR spectroscopy-based pressure sensor?" *İTÜ Surface Treatment Group*, pp. 1–5, 2022.
[36] H. Li and J. Watson, "Continuous glass fibers for reinforcement," in *Encyclopedia of Glass Science, Technology, History, and Culture*, P. Richet, R. Conradt, A. Takada, and J. Dyon, Eds., pp. 95–109, John Wiley & Sons, Ltd., 2021.
[37] L. Capriotti and A. Quaini, "High temperature behaviour of nuclear materials investigated by laser heating and fast pyrometry," *Master of Science in Nuclear Engineering*, 2012.
[38] F. C. Donnelly, F. Purcell-Milton, V. Framont, O. Cleary, P. W. Dunne, and Y. K. Gun'ko, "Synthesis of $CaCO_3$ nano- and micro-particles by dry ice carbonation," *Chemical Communications*, vol. 53, no. 49, pp. 6657–6660, 2017.
[39] S. Gunasekaran, G. Anbalagan, and S. Pandi, "Raman and infrared spectra of carbonates of calcite structure," *Journal of Raman Spectroscopy*, vol. 37, no. 9, pp. 892–899, 2006.
[40] N. Böhme, K. Hauke, M. Neuroth, and T. Geisler, "In situ Raman imaging of high-temperature solid-state reactions in the $CaSO_4$-SiO_2 system," *International Journal of Coal Science & Technology*, vol. 6, no. 2, pp. 247–259, 2019.
[41] J. Tatar, N. R. Brenkus, G. Subhash, C. R. Taylor, and H. R. Hamilton, "Characterization of adhesive interphase between epoxy and cement paste via Raman spectroscopy and mercury intrusion porosimetry," *Cement and Concrete Composites*, vol. 88, pp. 187–199, 2018.
[42] T. Schmid and P. Dariz, "Shedding light onto the spectra of lime: Raman and luminescence bands of CaO, Ca $(OH)_2$ and $CaCO_3$," *Journal of Raman Spectroscopy*, vol. 46, no. 1, pp. 141–146, 2015.
[43] F. A. Pisu, D. Chiriu, P. C. Ricci, and C. M. Carbonaro, "Defect related emission in calcium hydroxide: the controversial band at 780 cm^{-1}," *Crystals*, vol. 10, no. 4, Article ID 266, 2020.
[44] S. Ortaboy, J. Li, G. Geng et al., "Effects of CO_2 and temperature on the structure and chemistry of C–(A–) S-H investigated by Raman spectroscopy," *RSC Advances*, vol. 7, no. 77, pp. 48925–48933, 2017.